NON-LINEAR AEROELASTIC SIGNALS ANALYSIS USING TIME SERIES TECHNIQUES

Flávio Donizeti Marques, fmarques@sc.usp.br
Rui Marcos Grombone de Vasconcellos, ruivasc@sc.usp.br
Engineering School of São Carlos – University of São Paulo, Av. Trabalhador Sancarlense, 400, CEP 13566-590, São Carlos, SP, Brazil.

Abstract. *The application of time series analysis techniques for the analysis of non-linear aerolastic responses of an airfoil with trailing edge control surface is present in this work. Two elements typical section dynamics and a lumped vortex method for unsteady potential aerodynamics are considered to provide simulated aeroelastic data for the non-linear analysis. Concentrated freeplay nonlinearity is adopted to describe the restoring structural moment at control surface hinge, thereby allowing the introduction of a variety of complex behavior. Tests for stationarity and the Surrogate data test are followed by state space reconstruction. The Singular Value Decomposition method (SVD) and the method of Delays (MOD) are used to the state space reconstruction in order to show the diferences and potetiallity of each one. Reconstructed state spaces are, then, used in qualitative analysis of attractors evolution due to parametric variation concerned aeroelastic behavior. Lyapunov exponent calculation is proceeded, in order to search for chaos, that can be explored with Poincaré maps and bifurcation diagrams. This work results can also show how potentially useful are the application of time series analysis tools to the analysis of complex aeroelastic systems. Overall results reveal complex system dynamics. Poincaré mappings also suggest bifurcations and chaos, reinforced by the attainment of maximum positive Lyapunov exponents.*

Keywords: *nonlinear time series analysis, freeplay, state space reconstruction, chaos, control surface, typical section, aeroelastic*

1. INTRODUCTION

Non-linear behavior is inherent to aeroelastic systems and can be associated with aerodynamic and structural effects. An aeroelastic system can face both effects simultaneously or one of these at a time. Compressibility effects (Edwards, 1993) and highly separated flows (Leishman and Beddoes, 1989) are important effects that can result in nonlinear aerodynamical behavior, they can occur for instance, in transonic flight and high angles of attack manoeuvres, in all cases leading to complex models beyond linearity suppositions. In terms of structural properties, the effects of aging, loose attachments, material features, large motions or deformations are examples of non-linearities to be considered. Structural nonlinearities can be subdivided into distributed and concentrated ones. Distributed nonlinearities represents, for example, characteristic of materials and large motions (Patil and Hodges, 2004; Brown, 2003) as concentrated ones act locally, representing loose of attachments, worn hinges of control surfaces, aging and presence of external stores (Lee et al., 1999; O'Neil and Strganac, 1998; Bae et al., 2004; Conner et al., 1997; Tang and Dowell, 2006).

Non-linear systems typically present features like: multiple equilibrium points, bifurcations, limit-cycle oscillations and chaos (Sheta et al., 2002). The presence of such effects results in modifications in the aeroelastic behavior, leading to more laborious the prediction of instabilities. The flutter phenomenon with the presence of non-linearities, e.g., happens in a different way to that foreseen in linear models. Severe non-linear behavior can be encountered in aeroelastic systems with hinged control surfaces. A variety of undesired problems to the control surface hinge and links provides complex dynamic characteristics, which have a major influence on aeroelastic response. Typical aeroelastic models consider those control surface nonlinearities as concentrated effects, such as polynomial, free-play and hysteresis, or by a combination of these (Lee et al., 1999).

Techniques from signal processing and time series analysis can be used to analyze aeroelastic system (Shreiber and Shmitz, 2000; Kantz and Shreiber, 2004), thereby providing an powerful framework to explore complex non-linear fluid-structure interaction problems. Methodologies to reconstruct the state space from the embedded dynamics of a time series represent an appropriate approach to analysis aeroelastic systems. Bifurcations and chaotic behavior can be determined from reconstructed spaces. Moreover, systems invariants may also be calculated to check complex behavior, or to certify on the nonlinearity of the time series, as done by Simoni (2007); Marques et al. (2009); Marques and Vasconcellos (2009). In this cases, stationarity and surrogate data tests are performed, followed by state space reconstruction, Poincaré maps and Lyapunov exponents assessment, to explore bifurcations and chaotic behavior.

This work presents the application of time series analysis techniques for the analysis of non-linear aerolastic responses of an airfoil with trailing edge control surface. Two elements typical section dynamics and a lumped vortex method for unsteady potential aerodynamics are considered to provide simulated aeroelastic data for the non-linear analysis. Concentrated freeplay nonlinearity is adopted to describe the restoring structural moment at control surface hinge, thereby allowing the introduction of a variety of complex behavior. The method of Delays (MOD) is used to the state space

reconstruction. Reconstructed state spaces are then used in qualitative analysis of attractors evolution due to parametric variation concerned aeroelastic behavior. Lyapunov exponent calculation is proceeded, in order to search for chaos, that can be explored with Poincaré maps and bifurcation diagrams.

The Singular Value Decomposition method (SVD) is used to reconstruct the state space from a noise-contaminated time series to show its potentiality in experimental data. Some results obtained with time series analyses are compared with the results obtained directly from the mathematical model to show how potentially useful are the application of time series analysis tools to the analysis of complex aeroelastic systems, mainly when a mathematical model is not possible and we have only experimental data.

2. NONLINEAR AEROELASTIC MODEL

A two-dimensional airfoil having three degrees of freedom, as depicted in Fig.1, is investigated.

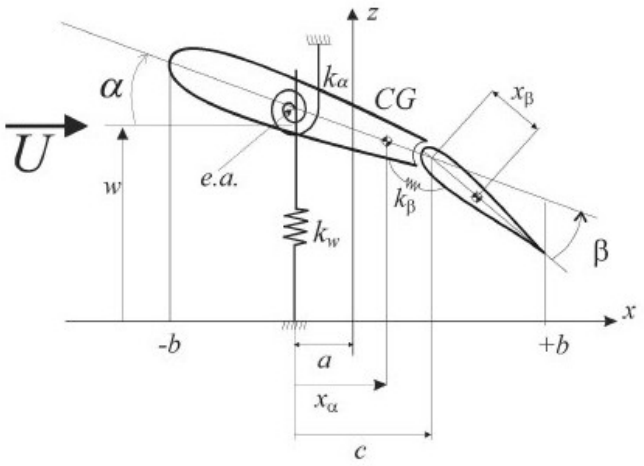

Figure 1. Structural representation of the aeroelastic model

The bending and torsion variables are denoted as w and α, respectively, and the control surface motion denoted by β. The bending deflexion w and the torsion α are measured at the elastic axis and the β angle of control surface is measured at the hinge line. In addition ab represents the distance from the elastic axis to midchord, c represents the distance between the elastic axis to the hinge line of control surface, b is the semichord of the entire airfoil section.

The mass center of the entire airfoil is located at a distance x_α from the elastic axis and the mass center of the control surface is located at a distance x_β from the hinge line, k_w represents the bending stiffness, k_α the stiffness of the torsion spring, k_β the stiffness of the control surface hinge and U the freestream velocity.

By using Lagrange's equation, the equations of motion of the typical section in Fig.1 are obtained. For details the reader can refer to technical literature Fung (1993). Here, the dimensionless form of the equation is expressed as,

$$\begin{bmatrix} 1 & -x_\alpha & -x_\beta \\ -x_\alpha & r_\alpha^2 & r_\beta^2 + x_\beta(c-a) \\ -x_\beta & r_\beta^2 + x_\beta(c-a) & r_\beta^2 \end{bmatrix} \begin{bmatrix} \ddot{w} \\ \ddot{\alpha} \\ \ddot{\beta} \end{bmatrix} + \begin{bmatrix} \omega_w^2 & 0 & 0 \\ 0 & r_\alpha^2\omega_\alpha^2 & 0 \\ 0 & 0 & r_\beta^2\omega_\beta^2 \end{bmatrix} \begin{bmatrix} w \\ \alpha \\ M(\beta) \end{bmatrix} = \frac{1}{mb^2} \begin{bmatrix} Lb \\ M_\alpha \\ H \end{bmatrix} \tag{1}$$

being

$$x_\alpha = \frac{S_\alpha}{mb};\ \ x_\beta = \frac{S_\beta}{mb};\ \ \omega_w^2 = \frac{k_w}{m};\ \ \omega_\alpha^2 = \frac{k_\alpha}{I_\alpha};\ \ \omega_\beta^2 = \frac{k_\beta}{I_\beta};\ \ r_\alpha^2 = \frac{I_\alpha}{mb^2};\ \ r_\beta^2 = \frac{I_\beta}{mb^2};$$

where, m is the mass of the entire system, I_α is the airfoil mass moment of inertia about the elastic axis, I_β is the control surface mass moment of inertia about the elastic axis; L and M_α are the aerodynamic lift and moment measured about the elastic axis and H is the aerodynamic moment on the flap about the flap hinge; S_α and S_β are the static mass moment, ω_w, ω_α and ω_β are the uncoupled natural frequencies.

A concentrated freeplay nonlinearity is assumed in the flap spring, to avoid problems with numerical instabilities, the freeplay discontinuity is represented by the tanh equation:

$$M(\beta) = \frac{1}{2}[1 - tanh(\varepsilon(\beta - \beta_l))](\beta - \beta_l) + \frac{1}{2}[1 + tanh(\varepsilon(\beta - \beta_u))](\beta - \beta_u) + f(\beta) \tag{2}$$

Where β_l and β_u are the lower and upper boundaries of the freeplay region respectively, $f(\beta)$ represents a preload upon the system and ε is a variable which determines the accuracy of the approximation, as ε tends to infinity, the approach tends to the real discontinuity. The Figure 2 shows the flap displacement β versus torque obtained with Eq. (2), $\beta_l = \beta_u = 0,5°$ and $\varepsilon = 4000$.

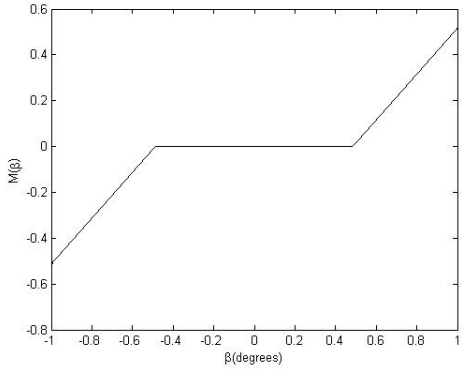

Figure 2. Flap displacement β versus torque obtained with Eq. (2), $\varepsilon = 4000$, $\beta_l = 0.5°$, $\beta_u = 0.5°$ e $f(\beta) = 0$

The solution of this aeroelastic system is strictly dependent of the aerodynamical model used to determine the unsteady aerodynamic loads L, M_α and M_β, in the right side of Eq. (1). The incompressible potential flow is assumed and the unsteady air loading over the airfoil is solved with the lumped vortex method (Katz and Plotkin, 2001). The thin-airfoil camberline is divided into N panels of the same length. A discrete vortex element is placed at the quarter chord of each panel, this point is called point vortex and the boundary conditions are observed at the tree-quarter chord point, called collocation point. At every time step, a new position of point vortices and collocation points of the control surface must be evaluated.

A lumped vortex model for a typical section is shown in Fig. 3. As the airfoil's circulation changes continuously, a continuous vortex sheet will be shed at the trailing edge, respecting Kelvin's condition. This continuous vortex sheet is approximated by a discrete-vortex wake model, whose vortex elements are represented by Γ_W. Two boundary conditions are defined: the zero normal velocity across body's solid boundaries and the flow disturbance, due to body motion through the fluid, should diminish far away from the body. Moreover, Kelvin and Kutta conditions have to be respected.

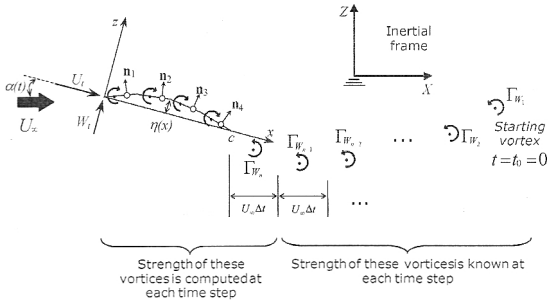

Figure 3. Discrete vortex model for the unsteady air loading calculation on the airfoil (Katz and Plotkin, 2001)

The induced velocities U_t and Wt at an arbitrary point (x, z) due to a vortex element Γ_j located at (x_j, z_j) is given by:

$$\left\{ \begin{array}{c} U_t \\ W_t \end{array} \right\} = \frac{\Gamma_j}{2\pi r_j^2} \left[\begin{array}{cc} 0 & 1 \\ 1 & 0 \end{array} \right] \left\{ \begin{array}{c} x - x_j \\ z - z_j \end{array} \right\} \tag{3}$$

where $r_j^2 = (x - x_j)^2 + (z - z_j)^2$ is the distance between the vortex element and the arbitrary point.

Considering the airfoil camberline divided into N panels, there will be N vortex elements at the N vortex points (x_j, z_j). The zero normal flow boundary condition will be fulfilled on the camberline at the collocation points i of each panel. The normal vector $\mathbf{n_i}$ at each of these collocation points are defined as:

$$\mathbf{n_i} = \frac{(-d\eta/dx, 1)}{\sqrt{(d\eta/dx)^2 + 1}} = (sin\alpha_i, cos\alpha i) \tag{4}$$

were α_i is the angle between panel i and local x axis,positive nose-up and $\eta(x)$ the surface shape.

An influence coefficient A_{ij} can be defined as the velocity component induced by the airfoil's or wake's j^{th} unit strength Γ_j, normal to the surface at the collocation point i. So, an algebraic equation can be obtained for each collocation point i, relating the influence coefficients, the vortex elements, they strength and the velocities induced by then into this collocation point. When the entire model is considered, the following set of equations is obtained.

$$\begin{bmatrix} A_{11} & A_{12} & \cdots & A_{1N} & A_{1W} \\ A_{21} & A_{22} & \cdots & A_{2N} & A_{2W} \\ \vdots & \vdots & \ddots & \vdots & \vdots \\ A_{N1} & A_{N2} & \cdots & A_{NN} & A_{NW} \\ 1 & 1 & \cdots & 1 & 1 \end{bmatrix} \begin{Bmatrix} \Gamma_1 \\ \Gamma_2 \\ \vdots \\ \Gamma_N \\ \Gamma_{Wt} \end{Bmatrix} = \begin{Bmatrix} RHS_1 \\ RHS_2 \\ \vdots \\ RHS_N \\ \Gamma(t - \triangle t) \end{Bmatrix} \tag{5}$$

where each line corresponds to one collocation point. Now, the right-hand side (*RHS*) terms are known at each time step and they are composed by the kinematics velocities due to the motion of the airfoil plus the velocity components induced by wake vortices, except the latest one. As the airfoil control surface position changes with time, the influence coefficients calculation has also to be done at each time step loop. The Kutta condition is not stated explicitly for the lumped vortex method and the Kelvin condition is represented by:

$$\Gamma(t) - \Gamma(t - \Delta t) + \Gamma_W = 0 \tag{6}$$

At each time step the strength of each discrete vortex is determined from the solution of the linear system of Eq. (6). The pressures and airloads are then computed by using the unsteady Bernoulli equation:

$$\frac{p_\infty - p}{\rho} = \frac{1}{2}\left[\left(\frac{\partial\phi}{\partial x}\right)^2 + \left(\frac{\partial\phi}{\partial y}\right)^2 + \left(\frac{\partial\phi}{\partial z}\right)^2\right] - \mathbf{v}.\nabla\phi + \frac{\partial\phi}{\partial t} \tag{7}$$

The total lift and moment are obtained by integrating the pressure difference between the camberline upper and lower surfaces along the chordline. At this point, all the terms necessary to the solution of Eq. (1) are known and it will be solved with the Runge-Kutta method.

3. TOOLS TO ANALYZE NONLINEAR TIME SERIES

This section presents some techniques that can be employed for the characterization of complex non-linear dynamics.

3.1 Tests to Stationarity and Surrogate data Test

It is suggested, as first steps toward nonlinear time series analysis, tests for stationarity and the surrogate data test to the time series. If a time series originates from a unknown process, it is important to investigate if the system parameters remain constant or not during the experiment and whether the data does or not does some non-linear deterministic dependencies (Parlitz, 1998).

Violations of the fact that the dynamical properties of the system underlying a signal must not change during the observation period can be checked simply by measuring them for several segments of the data set (Kantz and Shreiber, 2004). To investigate if the signal contains some non-linear deterministic dependencies, a surrogate data test can be useful. The basic idea with respect to the surrogate data technique is to make some hypothesis about the data and then try to contradict this hypothesis. A widely used hypothesis is that colored noise data is generated by a linear stochastic process. Therefore, the data are modified in such a way that the complete structure, except for the assumed properties, will be destroyed. This may be done by Fourier transforming the data and by randomly shuffling the phases, the power spectrum or equivalently, the autocorrelation function is not affected. A new time series, with the same power spectrum is obtained by transforming back into the time domain.

If the original data are just colored noise, estimators of dimension, average mutual information, Lyapunov exponents, prediction errors, etc... should give the same results for the original time series and the surrogates. If, however the analysis yields significant differences, the original data is more than "just noise" (Parlitz, 1998).

To improve the statistical robustness, several surrogates are generated. Furthermore, it is necessary to take into account a possibly static non-linear transformation of the data that would distort the Gaussian distribution of the assumed colored noise as done by Theiler et al. (1992).

3.2 State Space Reconstruction

State space reconstruction approaches use time histories, or time series $(\mathbf{s}(t))$, to extract the dynamics of a system. Reconstruction techniques are based on Taken's embedded theorem (Takens, 1981), which establishes that a time series $\mathbf{s}(t)$ has information on non-observable states. With $\mathbf{s}(t)$ it is possible to reconstruct the state space of the system comparable to the real case, preserving the invariants of the system, e. g., attractor dimension and Lyapunov exponents. This statement has been proven numerically by Takens (1981).

There are different methods for reconstruct the state space, like the *method of delays* (MOD) and the *singular value decomposition method* (SVD). The MOD is the most explored reconstruction method in the literature. In this technique a time delay (τ) and an embedding dimension (d) are required to generate delayed coordinates from time series $s(t)$ (Marques et al., 2006). If the time series is represented by the sequence $s[n], n = 1, 2, ...N$, where N is the total number of samples, and d is the embedding dimension, then the MOD reconstruction is given by

$$\mathbf{u}[n] = \{s[n], s[n+\tau], \ldots, s[n(d-1)\tau]\} \tag{8}$$

The delay τ can be determined by the average mutual information method (Fraser and Swinney, 1986) and the embedding dimension d by Cao (1997) method.

The reconstruction method based on singular value decomposition (SVD) has been proposed by Broomhead and King (1986). The methodology eliminates the need for a time delay parameter by using the properties of the covariance matrix of the data to generate uncorrelated coordinates. One of the advantages of SVD is the capacity of filtering the time series as a result of the reconstruction process. Kugiumtzis and Christophersen (1997) and Vasconcellos (2007) have compared MOD and SVD and they concluded that SVD is more reliable for noisy data (Casdagli et al., 1991; Vasconcellos, 2007). Therefore, in principle, the SVD approach is more suitable for experimentally acquired time series.

The SVD approach for state space reconstruction needs the covariance matrix constructed from data contained in the time series $s(t)$. In this case, each state of the system can be considered a statistical variable and the diagonalization of covariance matrix separates the states by their variance, allowing the assessment of the system dynamics from those states that have higher variance. As small variance states are dominated by noise, reconstruction is basically attained with filtering.

3.3 Poincaré sections and Lyapunov exponents

A powerful tool for the verification of complex dynamics, in particular, to identify chaotic patterns is Poincaré mapping. The key point is that this simplified geometry contains the essential information about the periodicity, quasi-periodicity, chaocity and bifurcations of the system dynamics (Hilborn, 2000). Bifurcation in this case, is the term used to describe any sudden change in the dynamics of the system due to the respective parametric change. Therefore, for any change on the attractor geometry with a parameter variation, bifurcations can be visualized by plotting one Poincaré section for each parameter value. The Poincaré section computation has been based on Merkwirth et al. (1998) and Kantz and Shreiber (2004), which proposes the section extracted directly from an embedded time series. The result is a set of (*n-1*)-dimensional vector points, used to perform an orthogonal projection.

Lyapunov exponents determination furnishes important indications with respect to chaotic patterns of dynamic systems. Lyapunov exponents describe the mean exponential increase, or decrease, of small perturbations on an attractor and are invariant with respect to diffeomorphic changes of the coordinate system (Parlitz, 1998). When the largest Lyapunov exponent is positive, the system is said to be chaotic. Direct methods to quantify the largest Lyapunov exponent estimate the divergent motion from the reconstructed space state, without fitting a model to the data.

The method proposed by Sato et al. (1987) considers the average exponential growth of the distance of neighboring orbits on a logarithmic scale via prediction error on the number of time steps k, that is,

$$p(k) = \frac{1}{Nt_s} \sum_{n=1}^{N} log_2\left(\frac{\|\mathbf{y}^{n+k} - \mathbf{y}^{nn+k}\|}{\|\mathbf{y}^{n} - \mathbf{y}^{nn}\|}\right) \quad , \tag{9}$$

where N is the number of data points, t_s is the sampling period, $\mathbf{y}^{nn}$ is the nearest neighbor of $\mathbf{y}^n$.

The dependence of the prediction error $p(k)$ on the number of time steps k may be divided into three phases. The transient, corresponding to the first phase, where the neighboring orbit converges to the direction corresponding to the largest Lyapunov exponent. The second phase, where the distance growths exponentially with $e^{(\lambda_1 t_s k)}$ until it exceeds the range of validity of the linear approximation of the flow around the reference orbit $\mathbf{y}^{n+k}$. Then, the last phase begins,

where the distance increases slower than exponentially until it decreases again due to foldings in the state space (Parlitz, 1998). If the second phase is sufficient long, a linear segment with slope λ appears in $p(k)$ *vs.* k plot. This slope value (λ) is associate with the Lyapunov exponent value. This also provides a direct verification of the exponential growth of distances to distinguish deterministic chaos from stochastic processes, where a *non*-exponential separation of trajectories occurs (Eckmann and Ruelle, 1985).

3.4 Results and Discussion

The mathematical model provides the time series $w(t)$, $\alpha(t)$, $\beta(t)$ and the respected velocities and accelerations. The parameters used in this analyses are listed in Tab 1.

Table 1. Parameters used during simulations

Parameter	value	Parameter	value
$\omega_w(rad/s)$	35	x_α	0.2
$\omega_\alpha(rad/s)$	42	x_β	0.0125
$\omega_\beta(rad/s)$	200	r_α	0.5
a	-0.4	r_β	0.079
c	0.6	μ	40
$b(m)$	0.15	$\rho(kg/m^3)$	1.225

The freeplay nonlinearity given by Eq. (2) is set with $\varepsilon = 4000$. The test cases for freestream speed and freeplay gap are listed in Tab 2. The Figure 4 show the output $\beta(t)$from the mathematical model.

Table 2. Test cases

fixed speed @ $18m/s$ freeplay gap (β_{lu}), in degrees
± 0.10
± 0.25
± 0.50
± 0.75
± 1.00

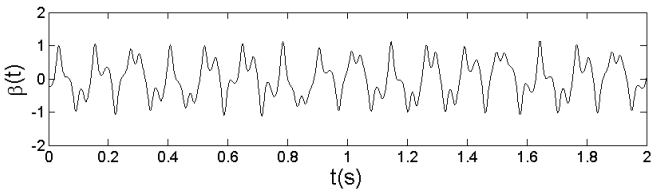

Figure 4. Time serie $\beta(t)$ from mathematical model, $U = 18m/s$), $\beta_{lu} = \pm 0.5°$

Each aeroelastic time series have been checked for stationarity with runtest and reverse arrangements test (Bendat and Piersol, 1986), prior to any analysis. All time series considered in this work have passed at the significance level of 0.05. In order to justify the use of non-linear analysis techniques, a surrogate data test was performed. Using the algorithm II of Theiler et al. (1992), 99 surrogates were generated and the correlation sum was computed for each by using the algorithm proposed by Grassberger and Procaccia (1983).

The Figure 5 presents the correlation sum of these 99 surrogates in the mean line with the error bars, the correlation sum computed for the SVD-filtered acquired data is present in the continuous line. Clearly, the data is out of correlation sum distribution generated for purely linear stochastic surrogate signal. This evidence reinforces that the signal may be representative of a deterministic nonlinear process. These results provide enough information to qualify further investigation using non-linear analysis tools

The state spaces are then reconstructed by MOD, from the time series $\beta(t)$ for each condition. The delay τ is determined by the Average Mutual Information method Fraser and Swinney (1986) and the embedding dimension d by Cao's method (Cao, 1997), embedding dimension 3 is found in all test cases. The Figure 6 presents the real state space, obtained directly from the model, the MOD-reconstructed state space from $\beta(t)$ and the SVD-reconstructed state space for the

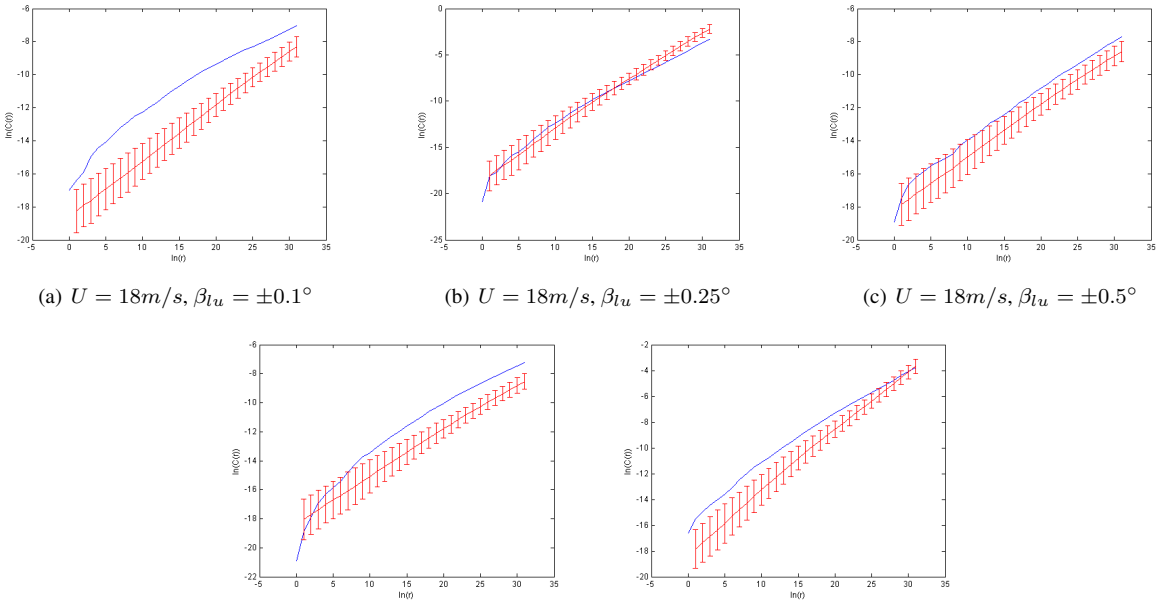

(a) $U = 18m/s$, $\beta_{lu} = \pm 0.1°$ (b) $U = 18m/s$, $\beta_{lu} = \pm 0.25°$ (c) $U = 18m/s$, $\beta_{lu} = \pm 0.5°$

(d) $U = 18m/s$, $\beta_{lu} = \pm 0.75°$ (e) $U = 18m/s$, $\beta_{lu} = \pm 1.0°$

Figure 5. Correlation Sum for $\beta(t)$ (blue) and the 99 surrogates (red), with $U = 18m/s$ and β_{lu} variating from $\pm 0.1°$ to $\pm 1.0°$

condition $U = 18m/s$), $\beta_{lu} = \pm 0.5°$. For the SVD reconstruction, Gaussian noise is addicted to the time series, with a sign-to-noise ratio ($SNR = 30$)

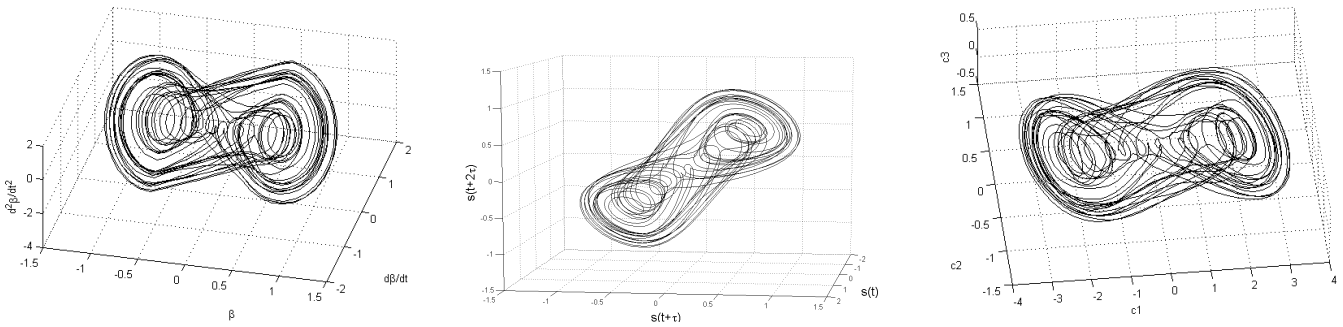

(a) Real state space (b) MOD reconstructed state space from $\beta(t)$ (c) SVD reconstructed state space from $\beta(t)$, $SNR = 30$

Figure 6. Real and reconstructed state spaces, $U = 18m/s$, $\beta_{lu} = \pm 0.5°$

As can be observed, the reconstructed state spaces are similar to the real one. The Figure 7 presents a projection of the real state space, here one can see that the control surface alternate between the extremes of freeplay, for this case $\beta_{lu} = \pm 0.5°$, in a complex pattern, possibly chaotic.

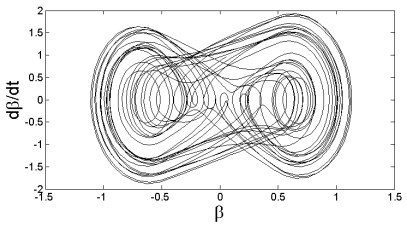

Figure 7. Bidimensional projection of the real state space

For the cases in Tab. 2, the reconstructed state spaces for each freeplay are plotted in Fig 8(a), the result is an evolution of trajectories in reconstructed state space due to freeplay variation. An amplitude increase in motion is observed,

moreover, changes in the shape of attractor can be observed, it suggest possible bifurcations.

In order to supply an easier visualization of the aforementioned transitions, or bifurcations. In Figure 8(b) one may observe considerable changes in the Poincaré sections as the freeplay increases, mainly between $\beta_{lu} = \pm 0.5°$ and $\beta_{lu} = \pm 0.75°$. Projected Poincaré sections, as illustrated in Figure 9(a), show an alternative way to visualize the bifurcations with respect to freeplay evolution.

The final step in the investigation of the complex non-linear behavior of the aeroelastic signals is the determination of the largest Lyapunov exponent. The Lyapunov exponents are computed for the Tab. 2 listed cases by the prediction error technique Sato et al. (1987) for the reconstructed state spaces and for real ones, to comparisons. The Figure 9(b) presents the procedure for one case and Tab. 3 summarize the results

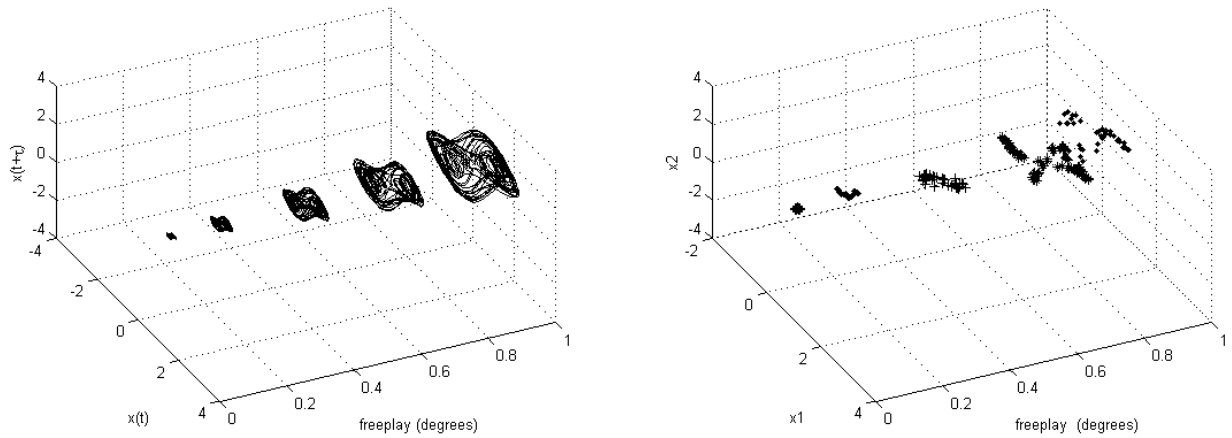

(a) State Space evolution (b) Poincaré section evolution

Figure 8. State Space and Poincaré section evolution due to freeplay increase

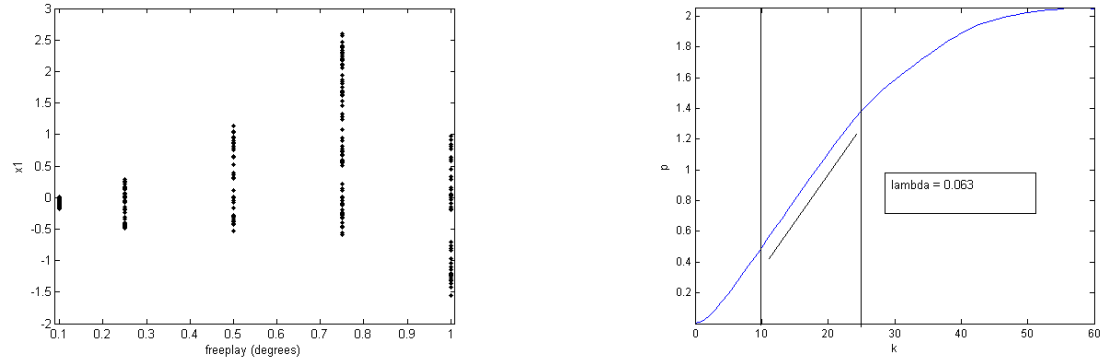

(a) Poincaré section projection evolution (b) Lyapunov exponent computation

Figure 9. Projected Poincaré section evolution due to freeplay increase and Lyapunov exponent computation: $U = 18m/s$ and $\beta_{lu} = \pm 0.5°$

Table 3. Lyapunov exponents computed for test cases by Sato et al. (1987) method

Fixed freestream speed @ $18m/s$		
freeplay (β_{lu}),in degrees	Lyapunov exponent (reconstructed)	Lyapunov exponent (real)
$\pm 0,10$	0.065	0.068
$\pm 0,25$	0.053	0.046
$\pm 0,50$	0.063	0.063
$\pm 0,75$	0.063	0.059
$\pm 1,00$	0.053	0.050

In all test cases, the Lyapunov exponent are positive, confirming the suspects that the motion is chaotic, moreover, the values computed for the real state spaces and the reconstructed are very close. The results show how potential are the time series analysis techniques presented in this work.

4. Concluding Remarks

Techniques from non-linear time series analysis theory were used in this work to investigate non-linear aeroelastic time series, from a mathematical model of a typical section with a concentrated freeplay nonlinearity at the control surface. The time series was tested for stationarity and for non-linearity by using the surrogate data method, in order to verify whether or not the data were representative of a non-linear process. The results has confirmed non-linear behavior, thereby justifying the application of non-linear techniques. The state spaces was reconstructed for a variety of test cases and the trajectories have revealed complex behavior, indicating bifurcations and chaos. The evolution with the freeplay increase suggests the occurrence of bifurcations, because changes in the shape of the attractor and Poincaré section have been observed. Finally, Lyapunov exponents were assessed and the results were positive Lyapunov exponents to each time series in the analysis, reinforcing the suspect of chaotic behavior, the values computed for the real state spaces and the reconstructed are very close.

5. ACKNOWLEDGMENTS

The authors acknowledge the financial support of the São Paulo State Research Agency, FAPESP (grant 2007/08459-1)

6. REFERENCES

Bae, J. S., D. J. Inman, and I. Lee (2004). Effects of structural nonlinearity on subsonic aeroelastic characteristics of an aircraft wing with control surface. *Journal of Fluids and Structures 19*, 747–763.

Bendat, J. S. and A. G. Piersol (1986). *Random Data: Analysis & Measurement Procedures* (Second ed.). New York: John Wiley & Sons.

Broomhead, D. S. and G. P. King (1986). Extracting qualitative dynamics from experimental data. *Physica D 20*, 217–236.

Brown, E. L. (2003). *Integrated Strain Actuation in Aircraft with Highly Flexible Composite Wings*. Ph. D. thesis, Massachusetts institute of Technology.

Cao, L. (1997). Practical method for determining the minimum embedding dimension of a scalar time series. *Physica D 110*, 43–50.

Casdagli, M., S. Eubank, D. Farmer, and J. Gibson (1991). State space reconstruction in the presence of noise. *Physica D 51*, 52–98.

Conner, M. D., D. M. Tang, and E. H. Dowell (1997). Nonlinear behavior of a typical airfoil section with control surface freeplay. *Journal of Fluids and Structures 1*(1), 89–109.

Eckmann, J. P. and D. Ruelle (1985). Ergodic theory of chaos and strange attractors. *Reviews of Modern Physics 57*, 617–656.

Edwards, J. W. (1993). Computational aeroelasticity. In A. K. Noor and S. L. Venner (Eds.), *Structural Dynamics and Aeroelasticity*, Volume 5 of *Flight Vehicle Materials, Structures and Dynamics - Assessment and Future Directions - ASME*, pp. 393–436.

Fraser, A. M. and H. L. Swinney (1986). Independent coordinates for strange attractors from mutual information. *Physical Review A 33*, 1134–1140.

Fung, Y. C. (1993). *An introduction to the theory of Aeroelasticity*. New York: Dover Publications.

Grassberger, P. and I. Procaccia (1983). Measuring the strangeness of strange attractors. *Physica D 9*, 189–208.

Hilborn, R. C. (2000). *Chaos and Nonlinear Dynamics: An Introduction for Scientists and Engineers;* (Second ed.). New York: Oxford U. Press.

Kantz, H. and T. Shreiber (2004). *Nonlinear Time Series Analisys* (Second ed.). Cambridge: Cambridge U. Press.

Katz, J. and A. Plotkin (2001). *Low-Speed Aerodinamics*. UK: Cambridge University Press.

Kugiumtzis, D. and N. Christophersen (1997, feb). State space reconstruction: Method of delays vs singular spectrum approach. Research Report 236, University of Oslo, Department of Informatics.

Lee, B. H. K., S. Price, and Y. Wong (1999). Nonlinear aeroelastic analysis of airfoils: bifurcation and chaos. *Progress in Aerospace Sciences 35*(3), 205–334.

Leishman, J. G. and T. S. Beddoes (1989). A semi-empirical model for dynamic stall. *Jornal of the American Helicopter Society 34*(3), 3–17.

Marques, F. D., E. M. Belo, V. A. Oliveira, J. R. Rosolen, and A. R. Simoni (2006). On the investigation of state space reconstruction of nonlinear aeroelastic response time series. *Shock and Vibration 13*, 393–407.

Marques, F. D. and R. M. G. Vasconcellos (2009). Chaotic patterns in aeroelastic signals. *Mathematical problems in Engineering*. Accepted for publication.

Marques, F. D., R. M. G. Vasconcellos, and A. R. Simoni (2009, March 2–6). Analysis of an experimental aeroelastic system through nonlinear time series. In *Proceedings of the International Symposium on Dynamic Problems of Mechanics – DINAME 2009*, Angra dos Reis, RJ, Brazil.

Merkwirth, C., U. Parlitz, and W. Lauterborn (1998, July 8–10). TSTOOL – a software package for nonlinear time series analysis. In J. A. Suykens and J. Vandewalle (Eds.), *Proceedings of the International Workshop on Advanced Black-Box Techniques for Nonlinear Modeling*, Katholieke Universiteit Leuven, Belgium.

O'Neil, T. and T. W. Strganac (1998). Aeroelastic response of a rigid wing supported by nonlinear springs. *Journal of Aircraft 35*(4), 616–622.

Parlitz, U. (1998). Nonlinear time-series analysis. In J. Suykens and J. Vandewalle (Eds.), *Nonlinear Modeling-Advanced black-box Techniques*, Boston, pp. 209–239. Kluwer Academic Publishers.

Patil, M. J. and D. H. Hodges (2004). On the importance of aerodynamic and structural geometrical nonlinearities in aeroelastic behavior of high-aspect-ratio wings. *Journal of Fluids and Structures 19*, 905–915.

Sato, S., M. Sano, and Y. Sawada (1987). Practical methods of measuring the generalized dimension and largest Lyapunov exponent in high dimensional chaotic systems. *Progress of Theoretical Physics 77*, 1–5.

Sheta, E. F., V. J. Harrand, D. E. Thompson, and T. W. Strganac (2002). Computational and experimental investigation of limit cycle oscillations of nonlinear aeroelastic systems. *Jornal of Aircraft 39*, 133–141.

Shreiber, T. and A. Shmitz (2000). Surrogate time series. *Physica D 142*, 346–382.

Simoni, A. R. (2007). *Análise de séries temporais esperimentais não lineares*. Ph. D. thesis, Escola de Engenharia de São Carlos - Universidade de São Paulo. (in portuguese).

Takens, F. (1981). Detecting strange attractors in turbulence. In D. Rand and L. Young (Eds.), *Dynamical Systems and Turbulence, Lecture Notes in Mathematics*, Volume 898, pp. 366–381. New York: Springer-Verlag.

Tang, D. and E. H. Dowell (2006). Flutter and limit-cycle oscillations for a wing-store model with freeplay. *Journal of Aircraft 43*(2), 487–503.

Theiler, J., B. Galdrikian, A. Longtin, S. Eubank, and J. D. Farmer (1992). Using surrogate data to detect nonlinearity in time series. In M. Casdagli and S. Eubank (Eds.), *Nonlinear Modeling and Forecasting*, Volume XII of *SFI Studies in the Sciences of Complexity*, Reading, MA, pp. 163–188. Addison-Wesley.

Vasconcellos, R. M. G. (2007). Reconstrução de espaços de estados aeroelásticos por decomposição em valores singulares. Master's thesis, Universidade de São Paulo - EESC-USP. (in portuguese).

7. Responsibility notice

The authors are the only responsible for the printed material included in this paper